T	absolute temperature, K
x_1, x_2	mole fractions, liquid phase
y_1, y_2	mole fractions, vapor phase

Registry No. Acetone, 67-64-1.

Literature Cited

(1) Coomber, B. A.; Wormald, C. J. *J. Chem. Thermodyn.* **1976**, *8*, 793.
(2) Loehe, J. R.; Van Ness, H. C.; Abbott, M. M. *J. Chem. Eng. Data* **1981**, *26*, 178.
(3) Winterhalter, D. R.; Van Ness, H. C. *J. Chem. Eng. Data* **1966**, *11*, 189.
(4) Van Ness, H. C.; Abbott, M. M. "Classical Thermodynamics of Nonelectrolyte Solutions: With Applications to Phase Equilibria"; McGraw-Hill: New York, 1982; pp 296-9, 348-55.
(5) Hayden, J. G.; O'Connell, J. P. *Ind. Eng. Chem. Process Des. Dev.* **1975**, *14*, 209.
(6) Reid, R. C.; Prausnitz, J. M.; Sherwood, T. K. "The Properties of Gases and Liquids", 3d ed.; McGraw-Hill: New York, 1977; p 632.
(7) Ambrose, D.; Sprake, C. H. S.; Townsend, R. *J. Chem. Thermodyn.* **1974**, *6*, 693.
(8) Kojima, K.; Tochigi, K.; Seki, H.; Watase, K. *Kagaku Kogaku* **1968**, *32*, 149.
(9) Verhoeye, L.; de Schepper, H. *J. Appl. Chem. Biotechnol.* **1973**, *23*, 607.

Received for review December 5, 1983. Accepted May 7, 1984. M.A.V. is grateful to the U.S.-Spanish Joint Committee for Scientific and Technological Cooperation for the award of a postdoctoral research grant.

Vapor/Liquid/Liquid Equilibrium and Heats of Mixing for Diethyl Ether/Water at 35 °C

Miguel A. Villamañán,† Ahmed J. Allawi, and Hendrick C. Van Ness*

Chemical and Environmental Engineering Department, Rensselaer Polytechnic Institute, Troy, New York 12180

Isothermal $P-x$ data and H^E data at 35 °C are reported for the system diethyl ether/water. These data are reduced to provide correlating expressions for G^E and H^E.

Liquid mixtures of diethyl ether and water exhibit partial miscibility. Available solubility data (none modern) are summarized by Sørensen and Arit (*1*); they show that at room temperature the solubility of ether in water is less than 2 mol % and decreases with increasing temperature, whereas the solubility of water in ether is about 5 mol %, increasing with increasing temperature. Useful data therefore require measurements in the dilute region of each species. Both the total-pressure vapor/liquid equilibrium (VLE) apparatus designed by Gibbs and Van Ness (*2*) and modified by DiElsi et al. (*3*) and the dilution calorimeter described by Winterhalter and Van Ness (*4*) are suitable for such measurements. However, one must be meticulous in making runs, and exercise patience, as equilibrium conditions are only slowly attained after mixing.

The anhydrous ethyl ether was HPLC grade supplied by Fisher Scientific Co. with minimum assay of 99.9 mol %. The water was doubly deionized with conductivity less than 1×10^{-6} Ω^{-1}. For VLE measurements, both reagents were thoroughly degassed. The measured vapor pressure of diethyl ether at 35 °C is 103.264 kPa compared with the value of 103.387 kPa reported by Ambrose et al. (*5*). For water, our value of 5.633 kPa compares with the value of 5.628 kPa reported by Ambrose and Lawrenson (*6*).

Results and Data Reduction

Vapor/Liquid/Liquid Equilibria. Table I contains experimental total-pressure data for the two regions of VLE. In the region of vapor/liquid/liquid equilibrium (VLLE), the observed three-phase equilibrium pressure is essentially constant, and measurements in this region establish this pressure as $P^\bullet$ = 104.70 ± 0.03 kPa.

For initial reduction of the two-phase equilibrium $P-x$ data, we make direct use of Barker's method (*7*), which is based on the following equilibrium equation:

$$P = x_1\gamma_1 P_1^{sat}/\Phi_1 + x_2\gamma_2 P_2^{sat}/\Phi_2 \qquad (1)$$

Table I. $P-x$ Data for Diethyl Ether (1)/Water (2) at 35 °C

x_1	x_2	P, kPa
0.0000	1.0000	5.633
0.0014	0.9986	18.759
0.0028	0.9972	33.033
0.0042	0.9958	45.083
0.0055	0.9945	57.298
0.0069	0.9931	68.679
0.0083	0.9917	79.064
0.0096	0.9904	89.632
0.0111	0.9889	100.205
	miscibility gap	
0.9536	0.0464	104.656
0.9617	0.0383	104.588
0.9715	0.0285	104.445
0.9818	0.0182	104.172
0.9901	0.0099	103.802
1.0000	0.0000	103.264

Here, the Φ_i are factors of order unity which take into account vapor-phase nonideality and the effect of pressure on liquid-phase fugacity. The γ_i reflect liquid-phase nonideality and are calculated from an assumed expression for G^E/RT. One determines by regression values of the parameters in this expression that minimize the sum of squares of the differences between the experimental values of P and those given by eq 1.

The $P-x$ data of Table I for both regions of VLE are well correlated by the modified Margules equation with a single set of parameters:

$$G^E/RT = \{A_{21}x_1 + A_{12}x_2 - \alpha_{12}\alpha_{21}x_1x_2/(\alpha_{12}x_1 + \alpha_{21}x_2)\}x_1x_2 \qquad (2)$$

From the resulting activity coefficients one then calculates the equilibrium y_i values for the regions of VLE:

$$y_i = x_i\gamma_i P_i^{sat}/(\Phi_i P) \qquad (3)$$

The results of this initial fit are represented by Figure 1. The intersections of both the $P-x$ curve and the $P-y$ curve for the VLE region dilute in ether with the three-phase-pressure line at $P^\bullet$ = 104.70 kPa are very sharp and allow us to establish unequivocal values of x_1^α, the lower miscibility limit, and $y_1^\bullet$, the three-phase vapor composition. Thus, we find that x_1^α = 0.01172 and $y_1^\bullet$ = 0.9463. The value of x_1^α may be compared with 0.0125 interpolated from the smoothed values given

† Permanent address: Dpto. de Termología, Facultad de Ciencias, Universidad de Valladolid, Valladolid, Spain.

0021-9568/84/1729-0431$01.50/0

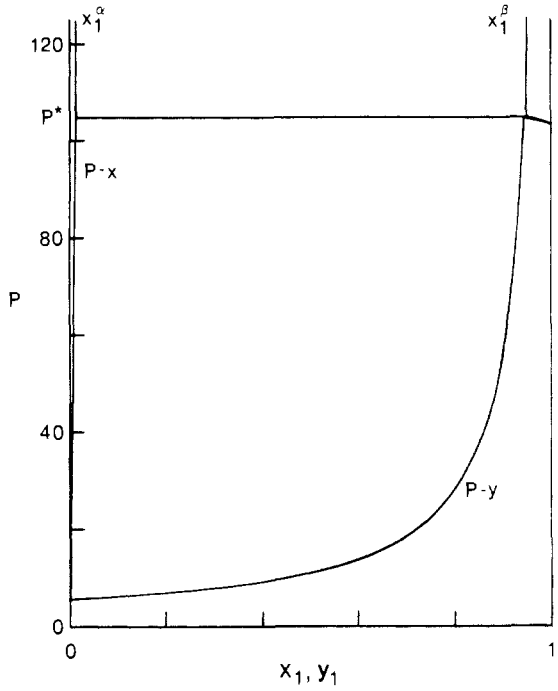

Figure 1. $P-y-x$ diagram for diethyl ether (1)/water (2) at 35 °C. Pressures are in kilopascals.

Table II. Summary of VLE and VLLE Results for Diethyl Ether (1)/Water (2) at 35 °C

A_{21}	3.35629
A_{12}	4.62424
α_{12}	3.76508
α_{21}	1.81775
rms δP, kPa	0.163
max $\|\delta P\|$, kPa	0.317
P^*, kPa	104.70
x_1^α	0.01172
x_1^β	0.9500
y_1^*	0.9463
B_{11}, cm^3/mol	−996
B_{22}, cm^3/mol	−1244
B_{12}, cm^3/mol	−567
V_1^L, cm^3/mol	107
V_2^L, cm^3/mol	18

by Sørensen and Arit (*1*). Although the location of the upper miscibility limit x_1^β is also mathematically established by this simple fitting procedure, its experimental location is uncertain because the intersection of the $P-x$ curve for the VLE region rich in ether with the three-phase-pressure line at $P^* = 104.70$ kPa is indistinct. Moreover, we have made no use of the equations for liquid/liquid equilibrium:

$$x_i^\alpha \gamma_i^\alpha = x_i^\beta \gamma_i^\beta \qquad (i = 1, 2) \tag{4}$$

With values of x_1^α, P^*, and y_1^* already fixed, we alter our fitting procedure so that it provides both a correlating equation for G^E/RT and a value of x_1^β that satisfy eq 4. Setting

$$Q \equiv \alpha_{12}\alpha_{21}x_1x_2/(\alpha_{12}x_1 + \alpha_{21}x_2) \tag{5}$$

we can write eq 2 as

$$\mathcal{G} \equiv G^E/(x_1x_2RT) = A_{21}x_1 + A_{12}x_2 - Q \tag{6}$$

whence

$$d\mathcal{G}/dx_1 = A_{21} - A_{12} - dQ/dx_1 \tag{7}$$

The activity coefficients are given by (*8*; eq 5-76)

$$\ln \gamma_1 = x_2^2\{\mathcal{G} + x_1(d\mathcal{G}/dx_1)\} \tag{8}$$

$$\ln \gamma_2 = x_1^2\{\mathcal{G} - x_2(d\mathcal{G}/dx_1)\} \tag{9}$$

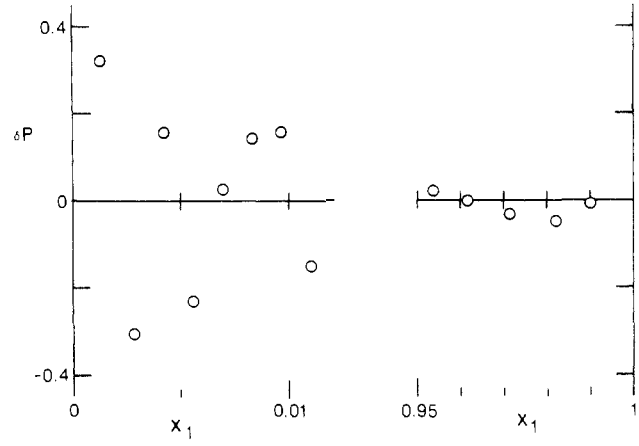

Figure 2. Pressure residuals (in kilopascals) for the two regions of VLE for diethyl ether (1)/water (2) at 35 °C.

Eliminating $\mathcal{G}$ and $d\mathcal{G}/dx_1$ from eq 8 and 9 by eq 6 and 7, solving simultaneously for A_{21} and A_{12}, and specializing the result to the miscibility limit denoted by superscript β gives

$$A_{21} = \{(x_1^\beta - x_2^\beta)/(x_1^\beta)^2\} \ln \gamma_2^\beta + (2/x_2^\beta) \ln \gamma_1^\beta + Q^\beta + x_2^\beta(dQ/dx_1)^\beta \tag{10}$$

$$A_{12} = \{(x_2^\beta - x_1^\beta)/(x_2^\beta)^2\} \ln \gamma_1^\beta + (2/x_1^\beta) \ln \gamma_2^\beta + Q^\beta - x_1^\beta(dQ/dx_1)^\beta \tag{11}$$

Equation 4 yields the following for LLE:

$$\ln \gamma_1^\beta = \ln \gamma_1^\alpha - \ln (x_1^\beta/x_1^\alpha) \tag{12}$$

$$\ln \gamma_2^\beta = \ln \gamma_2^\alpha - \ln (x_2^\beta/x_2^\alpha) \tag{13}$$

Eliminating $\ln \gamma_1^\beta$ and $\ln \gamma_2^\beta$ from eq 10–13, we get

$$A_{21} = \{(x_1^\beta - x_2^\beta)/(x_1^\beta)^2\}\{\ln \gamma_2^\alpha - \ln (x_2^\beta/x_2^\alpha)\} + (2/x_2^\beta)\{\ln \gamma_1^\alpha - \ln (x_1^\beta/x_1^\alpha) + Q^\beta + x_2^\beta(dQ/dx_1)^\beta \tag{14}$$

$$A_{12} = \{(x_2^\beta - x_1^\beta)/(x_2^\beta)^2\}\{\ln \gamma_1^\alpha - \ln (x_1^\beta/x_1^\alpha)\} + (2/x_1^\beta)\{\ln \gamma_2^\alpha - \ln (x_2^\beta/x_2^\alpha) + Q^\beta - x_1^\beta(dQ/dx_1)^\beta \tag{15}$$

In eq 14 and 15, γ_1^α and γ_2^α are given by

$$\gamma_i^\alpha = y_i^*\Phi_i P^*/(x_i^\alpha P_i^{sat}) \tag{16}$$

with Φ_i evaluated at the three-phase equilibrium conditions y_i^* and P^*. Thus, all quantities on the right of eq 16 have been established by the initial fit. Since $x_2^\beta = 1 - x_1^\beta$ and in view of eq 5, eq 14 and 15 relate the parameters A_{21} and A_{12} to the unknowns x_1^β, α_{12}, and α_{21}, and these quantities are now determined by a second regression based on all $P-x$ data for the two regions of VLE. This second step does not significantly degrade the quality of fit, nor does it lead to any inconsistency with the values of x_1^α, y_1^*, and P^* previously established. All pertinent results of the overall data-reduction process are listed in Table II, along with the ancillary data necessary for evaluation of Φ_i (*8*; eq 6-85). The values of A_{21} and A_{12} come from eq 14 and 15; the virial coefficients are calculated from the Hayden/O'Connell correlation (*9*). The value of 0.9500 for x_1^β is somewhat higher than 0.9425 interpolated from the values of Sørensen and Arit (*1*).

Figure 2 is a plot of pressure residuals; it indicates the quality of fit of the $P-x$ data in the two regions of miscibility. Figure 3 is a detailed view of the region of VLE for ether-rich mixtures. Note that the three-phase vapor composition y_1^* lies to the left of, but very close to, x_1^β. Thus, the system at 35 °C does not quite form a homogeneous azeotrope to the right of the upper miscibility limit.

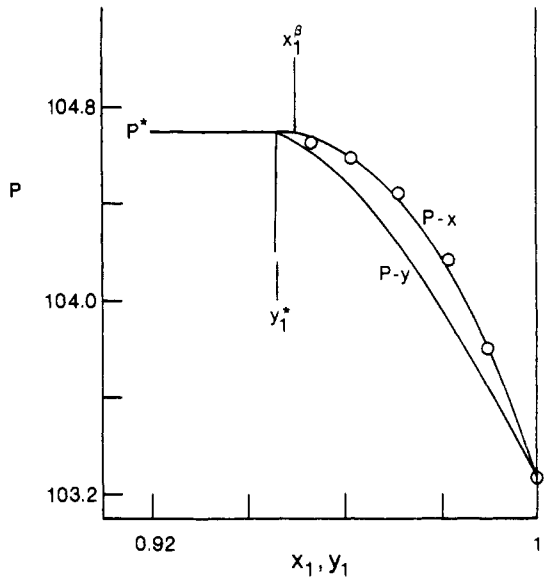

Figure 3. Detailed $P-y-x$ diagram for diethyl ether (1)/water (2) at 35 °C for ether-rich mixtures. Circles are $P-x$ data points. Pressures are in kilopascals.

Table III. H^E–x Data for Diethyl Ether (1)/Water (2) at 35 °C

x_1	x_2	H^E, J/mol
0.0029	0.9971	−43.9
0.0046	0.9954	−70.1
0.0063	0.9937	−93.8
0.0078	0.9922	−115.3
0.0117	0.9883	−158.8
	miscibility gap	
0.9526	0.0474	276.3
0.9555	0.0445	278.8
0.9664	0.0336	226.6
0.9688	0.0312	210.8
0.9731	0.0269	190.8
0.9800	0.0200	143.5
0.9850	0.0150	115.5
0.9876	0.0124	91.8

Table IV. Constants in Eq 29 for Temperature Dependence of Parameters in Eq 2

N_{ij}'	N_{ij0}
$A_{21}' = 3.36872$	$A_{210} = 22.66103$
$A_{12}' = -6.32214$	$A_{120} = -31.60533$
$C_{12}' = 14.00137$	$C_{120} = -392.96561$
$C_{21}' = -69.23038$	$C_{210} = 82.05381$

Heats of Mixing. Table III gives experimental H^E data for the two regions of miscibility at 35 °C. Correlation of all data is accomplished by the four-parameter Margules equation:

$$H^E/RT = (A_{21}'x_1 + A_{12}x_2)x_1x_2 - (C_{21}'x_1 + C_{12}'x_2)(x_1x_2)^2 \quad (17)$$

All of the H^E data at 35 °C are correlated with the parameter set given in the first column of Table IV; the rms δH^E is 3.72 J/mol. The quality of fit is indicated by Figure 4, where the function $\mathcal{H} \equiv H^E/(x_1x_2RT)$ is plotted vs. x_1. This function becomes indeterminate as either x_1 or x_2 approaches zero, and therefore the error bounds approach $\pm\infty$ at these limiting conditions. Thus, a plot of this function in the region of high dilution of one species magnifies error, and one expects scatter about the line representing the correlating equation. In contrast, the same data plotted as H^E vs. x_1 in Figure 5 display little scatter. Here, a few data points for the two-phase region are included. These must, of course, represent a continuous straight line across the diagram from one solubility limit to the other. The intersections of this straight line with the two branches of the correlating equation provide measures of the solubility limits, x_1^α and x_1^β. The value of x_1^α so indicated is consistent with the value determined from equilibrium measurements, whereas the indicated value of x_1^β is about 0.952, only slightly higher than the value found earlier by regression of the $P-x$ data.

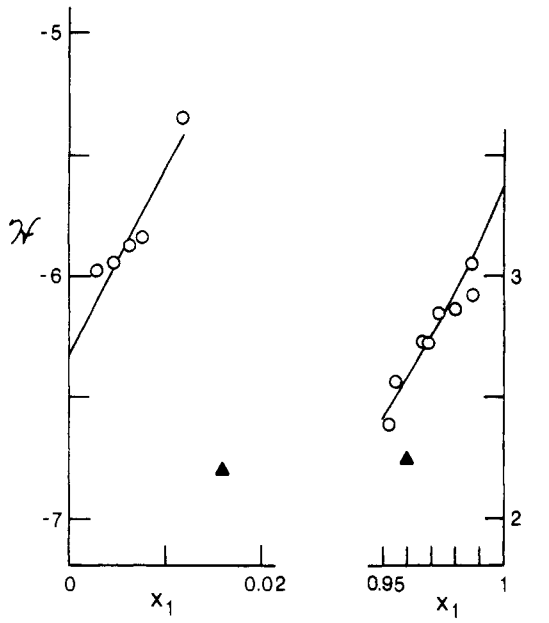

Figure 4. Plot of $\mathcal{H} \equiv H^E/(x_1x_2RT)$ vs. x_1 for the two regions of miscibility for diethyl ether (1)/water (2) at 35 °C. Circles are data points. The solid triangles represent the two values of Signer et al. (*10*) for the miscibility limits at 25 °C.

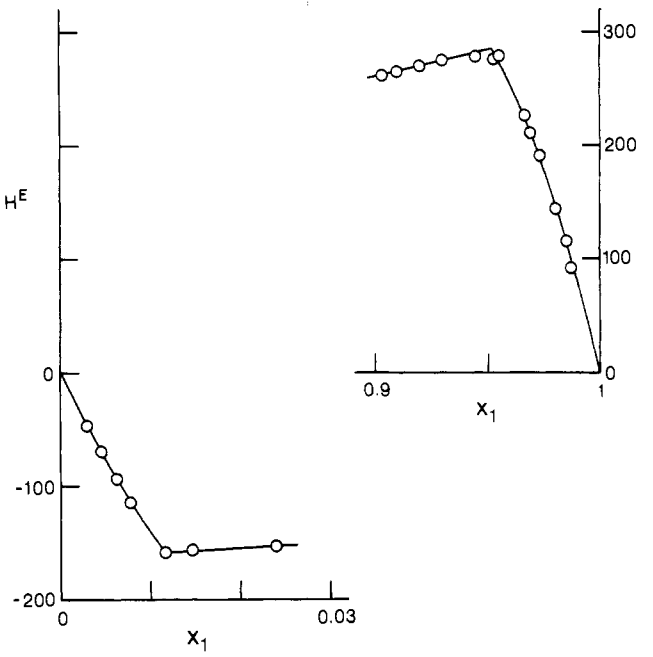

Figure 5. Plot of H^E (in J/mol) vs. x_1 for diethyl ether (1)/water (2) at 35 °C showing data points in the miscible and partially miscible regions.

Discussion

Signer et al. (*10*) report both H^E and VLLE data for diethyl ether/water at 25 °C. Their H^E data lie entirely between the miscibility limits and do indeed describe a straight line between these two points. Their two values at the miscibility limits have been converted to $\mathcal{H}$ values, and these are shown in Figure 4.

Since we have correlations for both G^E/RT and H^E/RT, we can calculate VLLE values at 25 °C for direct comparison with the data of Signer et al. However, we are unable to use the same correlating equation for both G^E/RT and H^E/RT, and it is therefore not obvious how we are to get the temperature dependence of the parameters in the equation for G^E/RT from the parameters in the equation for H^E/RT.

Consider first eq 17 written as

$$\mathcal{H} = A_{21}'x_1 + A_{12}'x_2 - (C_{21}'x_1 + C_{12}'x_2)x_1x_2$$

Differentiation at constant temperature gives

$$\partial\mathcal{H}/\partial x_1 = A_{21}' - A_{12}' - (C_{21}'x_1 + C_{12}'x_2)(x_2 - x_1) - x_1x_2(C_{21}' - C_{12}')$$

Whence

$$(\mathcal{H})_{x_1=1} = A_{21}' \quad (18)$$

$$(\mathcal{H})_{x_1=0} = A_{12}' \quad (19)$$

$$(\partial\mathcal{H}/\partial x_1)_{x_1=0} = A_{21}' - A_{12}' - C_{12}' \quad (20)$$

$$(\partial\mathcal{H}/\partial x_1)_{x_1=1} = A_{21}' - A_{12}' + C_{21}' \quad (21)$$

Similarly, one can show by eq 5-7 that

$$A_{21} = (\mathcal{G})_{x_1=1}$$

$$A_{12} = (\mathcal{G})_{x_1=0}$$

$$\alpha_{12} = A_{21} - A_{12} - (\partial\mathcal{G}/\partial x_1)_{x_1=0}$$

$$\alpha_{21} = A_{12} - A_{21} + (\partial\mathcal{G}/\partial x_1)_{x_1=1}$$

Whence at constant composition

$$\partial A_{21}/\partial T = (\partial\mathcal{G}/\partial T)_{x_1=1} \quad (22)$$

$$\partial A_{12}/\partial T = (\partial\mathcal{G}/\partial T)_{x_1=0} \quad (23)$$

$$\partial\alpha_{12}/\partial T = \partial A_{21}/\partial T - \partial A_{12}/\partial T - \partial(\partial\mathcal{G}/\partial x_1)_{x_1=0}/\partial T \quad (24)$$

$$\partial\alpha_{21}/\partial T = \partial A_{12}/\partial T - \partial A_{21}/\partial T + \partial(\partial\mathcal{G}/\partial x_1)_{x_1=1}/\partial T \quad (25)$$

By the Gibbs/Helmholtz equation (*8*; eq 5-61)

$$\partial\mathcal{G}/\partial T = -\mathcal{H}/T \quad (26)$$

and at constant temperature

$$\partial(\partial\mathcal{G}/\partial T)/\partial x_1 = -(\partial\mathcal{H}/\partial x_1)/T$$

This may equally well be written

$$\partial(\partial\mathcal{G}/\partial x_1)/\partial T = -(\partial\mathcal{H}/\partial x_1)/T \quad (27)$$

Appropriate combinations of eq 18-27 yield finally

$$\partial A_{21}/\partial T = -A_{21}'/T$$

$$\partial A_{12}/\partial T = -A_{12}'/T$$

$$\partial\alpha_{12}/\partial T = -C_{12}'/T$$

$$\partial\alpha_{21}/\partial T = -C_{21}'/T$$

Since each of these may be written

$$\partial M_{ij}/\partial T = -N_{ij}'/T \quad (28)$$

each may be integrated to give

$$M_{ij} = -N_{ij}' \ln T + N_{ij0} \quad (29)$$

where N_{ij}' has been assumed constant and N_{ij0} arises as an integration constant. Table IV lists these parameters as determined from the correlations already given for diethyl ether/water at 308.15 K. Parameters for the modified Margules equation for G^E/RT calculated from these values should give reasonable results for a temperature range at least from 290 to 330 K. For 298.15 K, we get

$$G^E/RT = 3.46742x_1 + 4.41567x_2 - (1.48118)(2.27965)x_1x_2/(1.48118x_1 + 2.27965x_2) \quad (30)$$

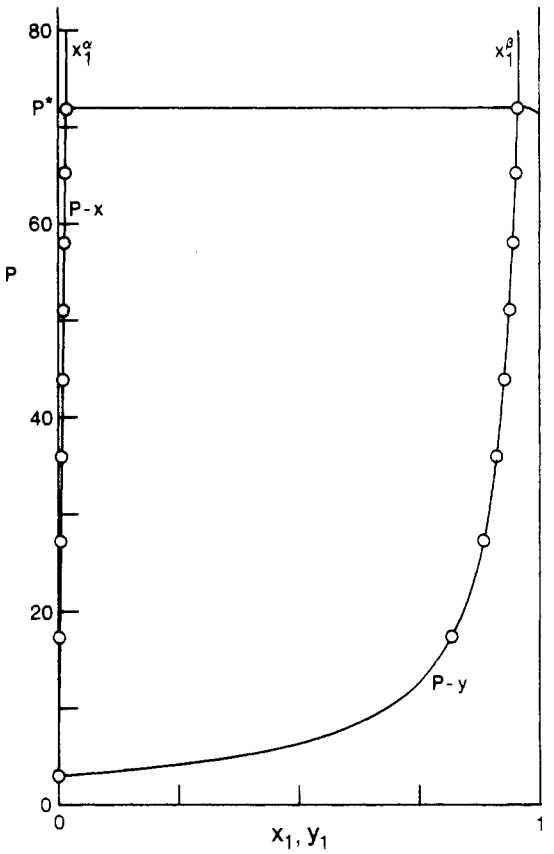

Figure 6. *P–x–y* diagram for diethyl ether (1)/water (2) at 25 °C. Lines are calculated from eq 30. Circles are the VLE data of Signer et al. (*10*) for the dilute-ether region. Pressures are in kilopascals.

With this equation we calculate P and y_1 as functions of x_1 for comparison with the data of Signer et al. (*10*) at 25 °C. We use their reported values of P_i^{sat} and virial coefficients from the Hayden/O'Connell correlation (*9*). Results are depicted by Figures 6 and 7. The former shows the full $P–x–y$ diagram with data points for the dilute-ether region of VLE. There is evident agreement of the experimental points with the calculated lines. However, because of the steepness of the $P–x$ and $P–y$ curves discrepancies in pressure of as much as 7 kPa occur, but this is equivalent to discrepancies in x_1 and y_1 of less than 0.002. Furthermore, the observed value of the lower solubility limit, $x_1^\alpha = 0.0159$, is significantly higher than the predicted value of 0.014 05.

Figure 7 is an enlarged view of the ether-rich region of VLE. The striking feature of this plot is the prediction of a homogeneous azeotrope at a mole fraction of about 0.96 and a pressure of about 71.96 kPa. The experimental data of Signer et al. are discrepant in this region, showing a change from $y_1 > x_1$ to $y_1 < x_1$ and indicating an azeotrope where $y_1 = x_1$. Moreover, the experimental value of y_1^* lies to the right of x_1^β, characteristic of the presence of an azeotrope. However, the experimental pressures fail to pass through a maximum and are most likely in error. Even so, errors of less than 0.1 kPa are indicated.

Comparison of Figures 3 and 7 shows that in going from 35 to 25 °C the ether/water system passes through a transition temperature below which it exhibits a homogeneous azeotrope and above which it does not. At this temperature the homogeneous azeotrope merges with the heterogeneous azeotrope,

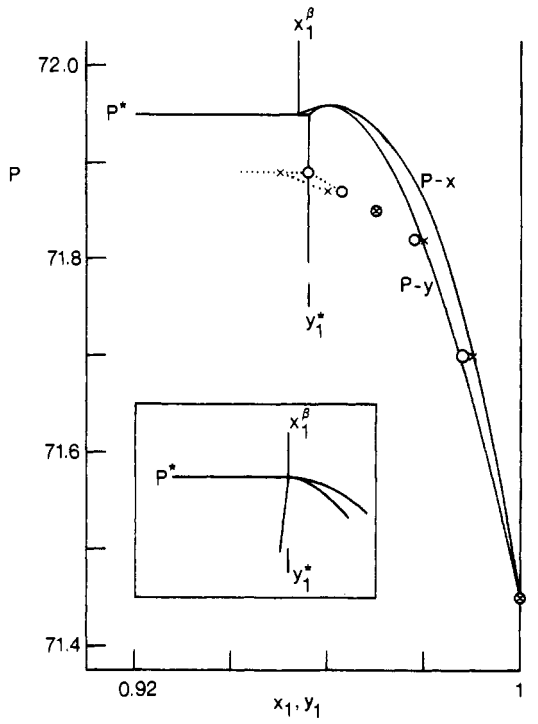

Figure 7. $P-x-y$ diagram for diethyl ether (1)/water (2) at 25 °C for the ether-rich region. Lines are calculated from eq 30. The circles are $P-y$ points and the x's are $P-x$ points from the VLE data of Signer et al. (*10*). Pressures are in kilopascals. The insert shows how the system behaves at the temperature of incipient homogeneous azeotropy.

and the right-hand branches of the $P-x$ and $P-y$ curves are tangent to the three-phase-pressure line. Moreover, these curves and the left-hand branch of $P-y$ curve all come together at the solubility limit x_1^β, as the sketch in the insert of Figure 7 shows.

Glossary

A_{12}, A_{21}	parameters in eq 2
A_{12}', A_{21}'	parameters in eq 17
B_{ij}	second virial coefficients
C_{12}', C_{21}'	parameters in eq 17
G^E	excess Gibbs energy
$\mathcal{G}$	$G^E/(x_1x_2RT)$
H^E	excess enthalpy
$\mathcal{H}$	$H^E/(x_1x_2RT)$
M_{ij}, N_{ij}', N_{ij0}	generic parameters, eq 29
P	total pressure
P^*	three-phase equilibrium pressure
P_i^{sat}	vapor pressure of pure i
Q	defined by eq 5
R	universal gas constant
T	absolute temperature
V_i^L	molar volume of pure liquid i
x_i	mole fraction, liquid phase
y_i	mole fraction, vapor phase
y_i^*	vapor-phase mole fraction for three-phase equilibrium

Greek Letters

α, β	as superscripts, identify values at miscibility limits
α_{12}, α_{21}	parameters in eq 2
γ_i	activity coefficient
δ	denotes the differences: calculated – experimental
Φ_i	correction factors in eq 1 and 3

Registry No. Diethyl ether, 60-29-7.

Literature Cited

(1) Sørensen, J. M.; Arit, W. "Liquid–Liquid Equilibrium Data Collection"; DECHEMA: Frankfurt/Main, West Germany, 1979; Chemistry Data Series, Vol. 5, Part 1, p 240.
(2) Gibbs, R. E.; Van Ness, H. C. *Ind. Eng. Chem. Fundam.* **1972**, *11*, 410.
(3) DIEIsi, D. P.; Patel, R. B.; Abbott, M. M.; Van Ness, H. C. *J. Chem. Eng. Data* **1978**, *23*, 242.
(4) Winterhalter, D. R.; Van Ness, H. C. *J. Chem. Eng. Data* **1966**, *11*, 189.
(5) Ambrose, D.; Sprake, C. H. S.; Townsend, R. *J. Chem. Thermodyn.* **1972**, *4*, 247.
(6) Ambrose, D.; Lawrenson, I. J. *J. Chem. Thermodyn.* **1972**, *4*, 755.
(7) Barker, J. A. *Aust. J. Chem.* **1953**, *6*, 207.
(8) Van Ness, H. C.; Abbott, M. M. "Classical Thermodynamics of Nonelectrolyte Solutions: With Applications to Phase Equilibria"; McGraw-Hill: New York, 1982.
(9) Hayden, J. G.; O'Connell, J. P. *Ind. Eng. Chem. Process Des. Dev.* **1975**, *14*, 209.
(10) Signer, R.; Arm, H.; Daeniker, H. *Helv. Chim. Acta* **1969**, *52*, 2347.

Received for review December 5, 1983. Accepted May 7, 1984. M.A.V. is grateful to the U.S.–Spanish Joint Committee for Scientific and Technological Cooperation for the award of a postdoctoral research grant.